



ELSEVIER

Journal of Crystal Growth 226 (2001) 231–239

JOURNAL OF
**CRYSTAL
GROWTH**

www.elsevier.nl/locate/jcrysgr

Float zone growth and characterization of $\text{Ge}_{1-x}\text{Si}_x$ ($x \leq 10$ at%) single crystals

T.A. Campbell^{a,1}, M. Schweizer^{a,c}, P. Dold^{a,*}, A. Cröll^b, K.W. Benz^a^aKristallographisches Institut, University of Freiburg, Hebelstrasse 25, D-79104 Freiburg i. Br., Germany^bInstitut für NE-Metallurgie und Reinststoffe, Technical University of Freiberg, Leipziger Str. 23, D-09599 Freiberg, Germany^cNASA, Marshall Space Flight Center SD47, Huntsville, AL 35812, USA

Received 17 January 2001; accepted 3 April 2001

Communicated by T. Hibiya

Abstract

$\text{Ge}_{1-x}\text{Si}_x$ ($x \leq 10$ at%) single crystals were grown with the float zone technique using a monoellipsoid mirror furnace. The feed rod consisted of pre-synthesized $\text{Ge}_{0.95}\text{Si}_{0.05}$ polycrystalline material with an initial composition of pure germanium. Several boron-doped ($1\text{--}2 \times 10^{17}$ at cm^{-3}) crystals were grown using $\langle 100 \rangle$ Ge seeds. Taking advantage of the pre-synthesized feed rods, a defined macrosegregation could be achieved in the grown crystals with a linear slope at the beginning (≈ 0.5 at% mm^{-1}) followed by a plateau region with a constant silicon distribution (Si concentration up to 10 at%, fluctuation rate: $\leq \pm 0.3$ at%). The etch pit density was in the range of $7 \times 10^3\text{--}2 \times 10^4$ cm^{-2} . Micrographs of the etched crystals show sharp changes in interface curvature at the crystal edges. These distortions of the interface morphology are a direct function of the Si concentration; they are considered to be caused by solutal Marangoni convection. Theoretical considerations show that the flow direction and strength vary significantly from a solutal Marangoni convection regime directly in front of the solid–liquid interface to a thermal Marangoni convection regime within the bulk melt. © 2001 Elsevier Science B.V. All rights reserved.

Keywords: A1. Computer simulation; A1. Convection; A1. Morphological stability; A1. Segregation; A1. Solutocapillary convection; A1. Thermocapillary convection; A2. Floating zone technique; B1. Germanium silicon alloys

1. Introduction

$\text{Ge}_{1-x}\text{Si}_x$ mixed crystals possess electrical properties which offer distinct advantages over pure silicon for certain applications. Within this

completely miscible system the bandgap increases with higher silicon concentration from a value of 0.72 to 1.2 eV. Applications are consequently feasible within both intrinsic and extrinsic photo-detectors, solar cells, gamma detectors, low temperature thermoresistors, high temperature thermoelectric generators, and substrate materials [1–4].

Dislocation-free $\text{Ge}_{1-x}\text{Si}_x$ single crystal growth is hindered by two issues: segregation and lattice mismatch. The Ge–Si system is a completely

*Corresponding author. Tel.: +49-761-203-6449; fax: +49-761-203-6434.

E-mail address: pit.dold@krist.uni-freiburg.de (P. Dold).

¹Research Fellow under the Alexander von Humboldt Foundation. Present address: Saint-Gobain Crystals & Detectors, 6801 Cochran Road, Solon, OH 44139, USA.

miscible system. Segregation coefficients vary from ≥ 0.3 on the Si-rich side to ≤ 5 on the Ge-rich side. Furthermore, critical compositional variations in the melt may arise from large differences in densities of the single elements in the liquid state ($\rho_{\text{Ge}} = 5.51 \text{ g cm}^{-3}$ [5] and $\rho_{\text{Si}} = 2.52 \text{ g cm}^{-3}$ [6]). Segregation is additionally exacerbated by high growth rates, compromising thermal equilibration and causing greater constitutional supercooling.

One recourse for $\text{Ge}_{1-x}\text{Si}_x$ growth is the float zone (FZ) technique. The main advantage of this method is the lack of wall contact; mechanical stress and contamination from the wall are thus eliminated. A disadvantage of $\text{Ge}_{1-x}\text{Si}_x$ grown by float zoning is the difficulty of feeding the base elements into the melt zone. Researchers have tried various means to prepare a $\text{Ge}_{1-x}\text{Si}_x$ feed rod. Saidov et al. [1] obtained single crystals less than 3 mm in diameter with up to 50 at% Ge by using pre-impregnated silicon ingots. Wollweber et al. [7,8] investigated Si-rich charge compositions with $x = 0.78-1$ and obtained high quality single crystals from 13 to 32 mm in diameter by depositing Ge granules through a hole in the feed rod into the melt. At present, there is only one earlier publication [9] known to the authors which demonstrates single crystal FZ growth on the Ge-rich side of the phase diagram.

The influence of Marangoni convection on the mass and heat transport has to be considered when growing crystals by the FZ technique [10–13]. Whereas the temperature dependence of the surface tension is primarily investigated as the driving source for convective flow, there are also a few papers examining the interaction of thermocapillary and solutocapillary convection, i.e., the flow driven by the concentration dependence of the surface tension. Using NaNO_3 as a transparent model liquid, Schwabe et al. [14] proved that the flow direction may change if they inserted a certain organic additive which alters the surface tension. Arafune et al. [15,16] demonstrated recently in a horizontal model arrangement for the Ga–In–Sb system that solutal Marangoni convection can cause flow velocities more than twice as high than thermal Marangoni convection. Tison et al. [17] observed a second, counter-rotating flow roll ahead

of the solidification front if they added bismuth to a tin melt. The results were confirmed by Kaddeche et al. [18] through numerical simulations.

The experiments presented in this article concern the Ge-rich side of the phase diagram. Main emphasis is put on segregation effects, the control of the initial concentration increase, reduction of the etch pit density (EPD), and the influence of thermal and solutal convection on axial and radial silicon distribution profiles as well as on the morphology of the solid–liquid interface.

2. Experimental procedure

To gradually incorporate silicon into a germanium melt during FZ growth is a design challenge. In monoellipsoid mirror furnaces it is necessary to contain the germanium–silicon alloy in a sealed quartz ampoule to fix the feed rod and to maintain sample purity (gas atmosphere: 700 mbar Ar + 100 mbar H_2). The advantage of the mirror furnace is the optical access to the liquid zone which makes it easy to control the height of the liquid zone. Furthermore, the temperature profile is characterized by a homogeneous, axisymmetric distribution. The use of sealed quartz ampoules precludes active mechanical introduction of silicon or germanium pellets into the melt as was done by Wollweber et al. [7]. Thus, germanium–silicon feed rods of an average concentration of 5 at% Si were pre-synthesized in pBN-crucibles using a high temperature resistance furnace. The introduction of boron from the crucible into the $\text{Ge}_{1-x}\text{Si}_x$ material during the synthesis cannot be avoided; doping levels were in the range of $1-2 \times 10^{17} \text{ at\% cm}^{-3}$ [19]. Fig. 1 shows the growth set-up and a typical silicon distribution profile of the pre-synthesized feed material.

A total of 13 growth experiments were performed. Table 1 presents the test matrix. The charge lengths and diameters are dictated by the maximum feasible dimensions possible within the radiation heated FZ configuration. Measurements of axial temperature profiles in specially prepared cartridges (using a Pt/PtRh-thermocouple, protected by an alumina capillary and capable of axial

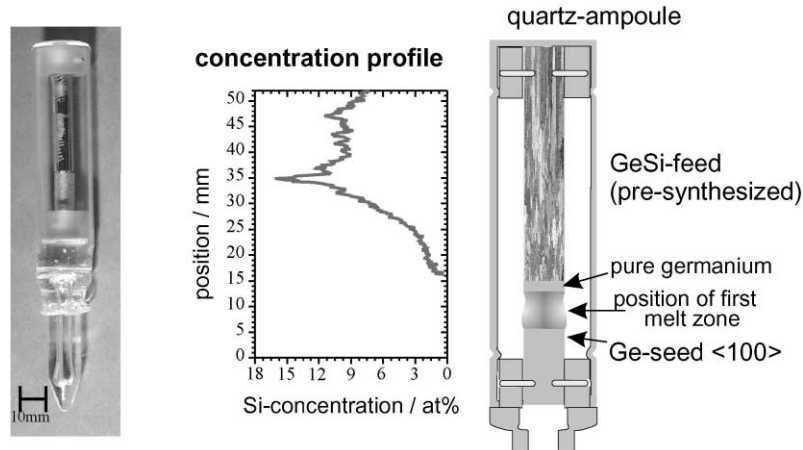


Fig. 1. Ampoule arrangement and silicon distribution of the pre-synthesized feed rod.

Table 1
Test matrix for the float zone experiments

| Variable | Value |
|----------------------------------|--|
| Sample dimensions (mm) with seed | Length = 85 diameter = 8 |
| Maximum growth length (mm) | 44 |
| Translation rate (mm/h) | 0.5–2.0 |
| Rotational rate (rpm) | 0 or 2 |
| Seed | <100> oriented $\rho \geq 50 \Omega \text{ cm}$ |

translation) showed temperature gradients at the solid–liquid interface of 20 K cm^{-1} and an axial temperature difference within the liquid zone of 6°C . The 0.5 mm h^{-1} translation rate was chosen based on the Tiller criterion [20,21]. Pure germanium seeds were used in all experiments; a <100> orientation was chosen to minimize radial segregation from facet formation.

A general description of the monoellipsoid mirror furnace may be found in Refs. [11,22]. Crystals were cut perpendicular to the <100> seed (parallel to the (110) plane) to investigate the axial segregation profile with regard to the silicon content. Details of the sample treatment and the crystal characterization are given in Ref. [23].

3. Results and discussion

3.1. Macrosegregation

The axial segregations of the FZ crystals as well as the directionally solidified feed rods were measured by line scans along the growth axis with an energy dispersive analysis by X-ray (EDAX) system. A segregation profile close to complete convective mixing conditions during the feed rod's synthesis allowed the use of a smoothly increasing axial gradient of the silicon concentration: the ends of the synthesized rods were used as the beginning of the feed rod for the FZ process. Therefore, growth started without silicon and resulted in a maximum silicon concentration in the single crystals of approximately 10 at%. All crystals show a smooth incorporation of silicon into the growing crystal as to be expected from the feed rod concentration profiles. The initial slope is nearly linear (Fig. 2) with a value of approximately 0.5 at% mm^{-1} over a range of 10–20 mm, and ends in a plateau region with constant silicon concentration. The length of the plateau is limited by the geometry of the furnace. In Fig. 2, a plateau of approximately 10 mm was achieved, with a Si concentration of 7.7 at% and a deviation of $\pm 0.3 \text{ at%}$. Radial macrosegregation reflects the slightly convex curvature of the interface: in the

“slope region”, the silicon concentration increases from the center to the edge by about 0.5 at%. This can be explained by the axial concentration gradient (i.e., the outer parts are grown at a later time than the center parts). In the plateau region, radial macrosegregation cannot be resolved by EDAX.

3.2. Etch pit densities

Average seed EPD was determined to be in the range of 2.4×10^4 – $2.9 \times 10^4 \text{ cm}^{-2}$. After the seed, there is a peak in the EPD most probably caused by back-melting and growth initiation. After initial zone establishment, the EPD settled into a range of 7×10^3 – $2 \times 10^4 \text{ cm}^{-2}$. In comparison to vertical Bridgman (VB) grown samples (in this

case, crystal orientation was [111]) of similar diameter and silicon concentration, the dislocation density for FZ crystals is considerably diminished. Dold et al. [23] reported an EPD range from 6×10^4 to $1 \times 10^5 \text{ cm}^{-2}$ in their VB grown crystals after the initial peak from seeding. Fig. 3 shows the axial profile of the EPD of an FZ grown crystal together with the distribution within a VB grown $\text{Ge}_{1-x}\text{Si}_x$ crystal [23]. Furthermore, VB grown crystals exhibit an enhanced dislocation density at the points of wall contact (see Fig. 4 in Ref. [23]), with EPD's higher than 10^6 cm^{-2} . FZ crystals on the other hand have no wall contact, and thus the EPD at the crystal outer edge is uniform and small in comparison. The influence of the different crystal orientation will be subject to further investigations.

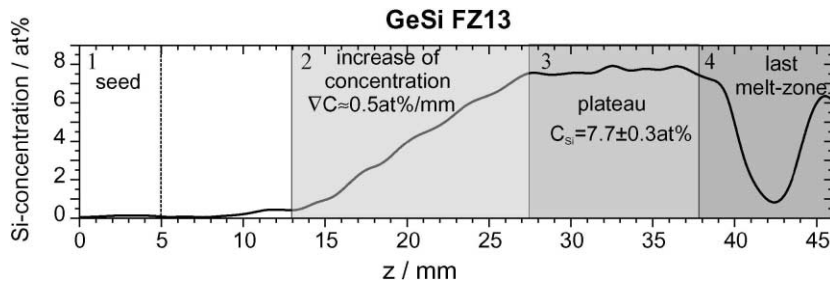


Fig. 2. Axial segregation profile: Growth started with pure germanium. Due to the silicon distribution in the feed rod, a linear increase of the silicon and a constant plateau was achieved.

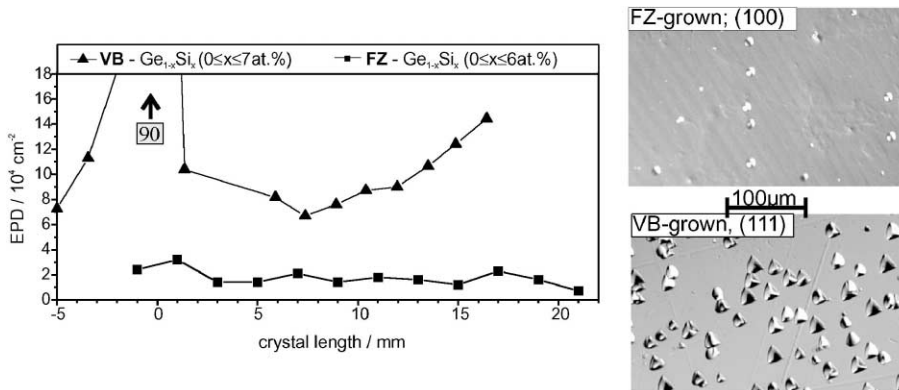


Fig. 3. Axial EPD of a float zone grown crystal compared to a crystal grown by the vertical Bridgman technique (left-hand side) and corresponding parts of radial wafers (right-hand side). The axial profile as well as the cross sections show the EPD of the central part of the crystal. In the periphery, the EPD increases considerably in the case of the Bridgman grown sample but remains constant in the case of the float zone one.

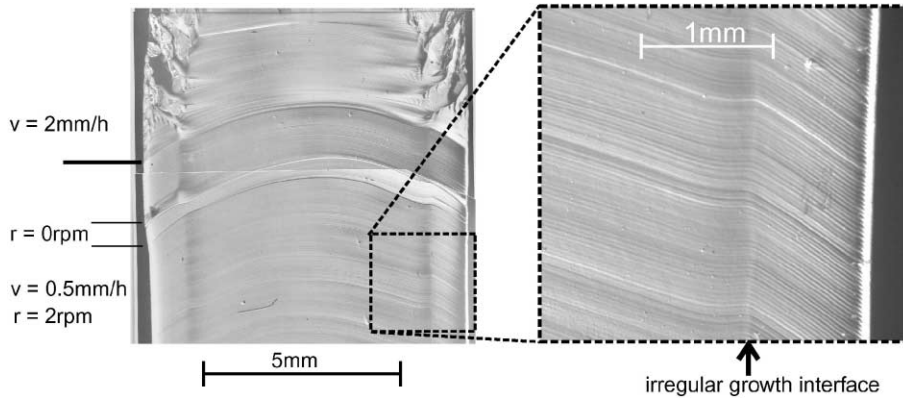


Fig. 4. Part of a topogram of an etched axial crystal (observed by Nomarski Interference Contrast Microscopy). In the periphery, a deviation from the convex interface shape occurs.

3.3. Interface morphology

One immediately noticeable feature in the micrographs of the etched samples is the edge curvature in the interface morphology which develops in the $\text{Ge}_{1-x}\text{Si}_x$ crystals (Fig. 4). This sharp change of the interface curvature increases in magnitude with increasing silicon concentration; digitized interface shapes as a function of the silicon concentration are plotted in Fig. 5. The maximum deviation from the (extrapolated) convex interface was determined to $\Delta z = 115 \mu\text{m}$ (see Fig. 5). This change in the morphology is not related to:

1. crystal orientation (and therefore not to the formation of growth facets because only $\langle 111 \rangle$ facets are formed in germanium); the same curvature was observed in polycrystalline material.
2. seed or feed rotation; during the growth process of the crystal GeSi-FZ10 the rotation was stopped for 1 h, but the interface distortion remained.

On the other hand, a clear relation is seen with respect to:

1. the presence of a free melt surface; the effect of the interface disturbance was not observed in over 40 Bridgman grown samples.

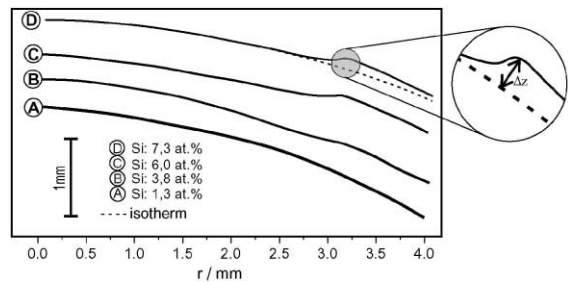


Fig. 5. Interface shape as a function of silicon concentration ($r = 4.0 \text{ mm}$ corresponds to the crystal edge). The dotted line in curve D is the extrapolated “normal shape”, following the solid–liquid isotherm. For a Si concentration of 7.3 at%, a maximum deviation from the isotherm of $\Delta z = 115 \mu\text{m}$ was measured, located at a radial position $r = 3.1 \text{ mm}$.

2. the amount of silicon in the melt, as already pointed out in Fig. 5. Disturbances could not be detected for Si concentrations smaller than approximately 2 at%. Additionally, a regular convex interface shape was obtained in a gallium-doped, silicon-free germanium FZ crystal grown as a reference sample under identical growth conditions.

Thus, we suspect the interface edge curvature may be caused by concentration-dependent (solutal) convection; it might be either solutal buoyancy or solutocapillary convection (or their superposition). In the axial direction, we obtain a stable density layering due to the segregation coefficient of silicon

greater than 1 (i.e., an enrichment of the more dense germanium takes place at the interface). Nevertheless, radial gradients are present. Even if the interface curvature is more convex in the case of FZ-grown crystals compared to Bridgman grown ones, the fact that this kind of interface disturbance was not observed in any of the Bridgman samples indicates that solutocapillary convection related to the free melt surface plays the dominant role.

The change in the interface morphology is not related to significant radial segregation. Neither EDAX nor WDX (Wave Length Dispersive Analysis by X-ray) measurements indicated a substantial change in the radial concentration profile. Assuming the interface followed the iso-concentration line and the isotherms were not disturbed and followed the dotted line in Fig. 5, a Δz of $115\ \mu\text{m}$ corresponds to a $\Delta T = 0.23^\circ\text{C}$ (with a temperature gradient at the interface of $\nabla T = 20\ \text{K cm}^{-1}$, cf., Section 2) between the isotherm of the undisturbed interface and the interface in the periphery. According to the phase diagram, this corresponds to a concentration difference of $\Delta C = 0.1\ \text{at}\%$, which is below the detection limit. On the other hand, when we increase the pulling rate to values which violate

the stability criterion for a stable interface, the growth instability starts within these edge structures and macrosteps form first within this 1 mm wide area in the vicinity of the free surface. Fig. 6 shows the magnified part of a crystal where morphological instabilities occurred. The spatially resolved microscopic growth velocity was measured in the center and in the periphery. The microscopic growth rate was obtained by measuring the distance from one rotational striation to the next one. In the center part a smooth transition from 0.5 to $2\ \text{mm h}^{-1}$ is observed; the transient region extends over $\approx 30\ \text{min}$ until the equilibrium is reached again. In the periphery, the microscopic growth rate exceeded the pulling speed by a factor of 1.5 and reached values of $3\ \text{mm h}^{-1}$, followed by a sharp reduction of the growth velocity. This indicates that the solutocapillary convection can destabilize the growth front and has to be taken into account as a potential source for interface breakdown.

3.4. Order of magnitude analysis of thermo- and solutocapillary convection

Due to the large segregation coefficient of Si in Ge of $k_0 \leq 5$, germanium is enriched in front of the

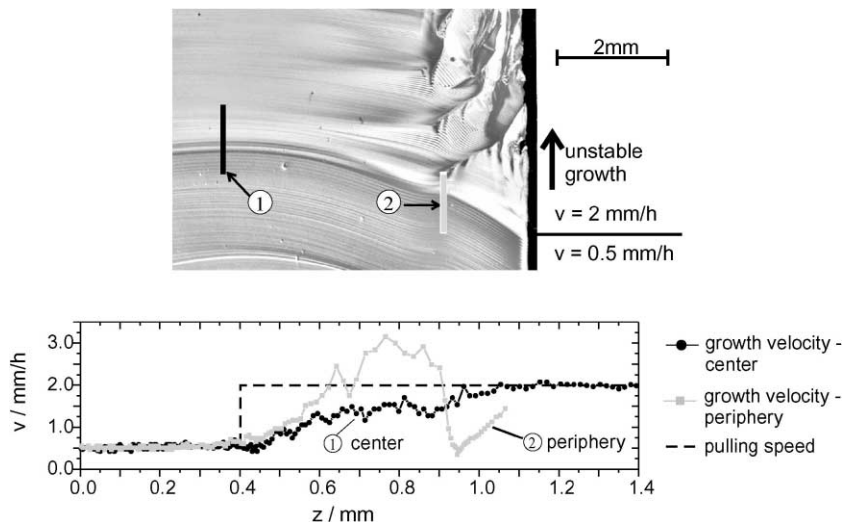


Fig. 6. Increasing the pulling speed to values above the stability criterion, interface breakdown starts within the boundary edge (top). The microscopic growth velocity changes smoothly in the center part of the crystal but irregularly in the peripheral part (bottom).

Table 2

Physical properties and resulting dimensionless characteristic numbers for liquid germanium and silicon at their melting points. If not indicated otherwise, values are taken from Table 1 in Ref. [24] which is based on Refs. [5,29]

| Variable | Si | Ge |
|---|----------------------|-----------------------------------|
| Diffusion constant, D ($\text{cm}^2 \text{s}^{-1}$) | 3×10^{-4} | 0.6×10^{-4} |
| Kinematic viscosity, ν ($\text{cm}^2 \text{s}^{-1}$) | 0.0035 | 0.00135 |
| Thermal diffusivity, κ ($\text{cm}^2 \text{s}^{-1}$) | 0.13 [30] | 0.175 |
| Density, ρ (g cm^{-3}) | 2.52 [31] | 5.51 |
| Surface tension, γ (N m^{-1}) | 0.72–0.88 [30,32,33] | 0.60 [34], 0.617 [35], 0.621 [24] |
| Temperature dependence of surface tension, $\partial\gamma/\partial T$ ($\text{mN m}^{-1} \text{K}^{-1}$) | – 0.28 [32] | – 0.08 [25] – 0.12 [34] |
| Prandtl number, $\text{Pr} = \nu/\kappa$ | 0.027 | 0.008 |
| Schmidt number, $\text{Sc} = \nu/D$ | 11 | 22 |

interface. As a consequence of the Schmidt number being much larger than the Prandtl number (see Table 2), the solutal boundary layer is significantly smaller than the thermal one. Calculation of δ_c by the equation given in Ref. [24] results in a boundary layer of $\delta_c \leq 1$ mm. To determine the concentration and the temperature dependence of the surface tension, sessile drop measurements have been used [25]. $\partial\gamma/\partial C$ was measured to $+2.2 \text{ mN m}^{-1} \text{ at\% Si}$, determined for $\text{Ge}_{1-x}\text{Si}_x$ melts with $0 \leq x \leq 13$ at% Si [26,27]. This is in good agreement with a linear interpolation between the surface tension values of pure Si and Ge (see Table 2) as well as with literature values given for intermediate compositions [28]. Combining this with the high segregation coefficient of Si in Ge leads to a profile with the lowest surface tension directly at the interface and an increase toward the center of the free surface. The surface tension gradient due to the temperature distribution, however, results in a profile with the highest value at both interfaces and the minimum at the zone center.² These competing mechanisms are of particular importance since they indicate that opposing flow rolls may occur: the thermocapillary component drives the fluid toward the solid–liquid interface and the solutocapillary component leads to an inverse flow away from the interface. Which one dominates at a given

coordinate depends on the value of the combined axial surface tension gradient:

$$\frac{\partial\gamma}{\partial z} = \frac{\partial\gamma}{\partial T} \frac{\partial T}{\partial z} + \frac{\partial\gamma}{\partial C} \frac{\partial C}{\partial z}. \quad (1)$$

We know from the experimental findings that we are close to the limit for constitutional supercooling; therefore, according to Tison et al. [17], the concentration gradient can be expressed as a function of the temperature gradient and the slope of the liquidus curve m_L :

$$\frac{\partial C}{\partial z} \leq \frac{\partial T}{\partial z} \frac{1}{m_L}. \quad (2)$$

In the range of 2–10 at% silicon, the slope of the liquidus curve is approximately 9 K at\%^{-1} , giving $0.22 \text{ at\% mm}^{-1}$ for the concentration gradient. Therefore in the solute boundary layer the solutal contribution $\partial\gamma/\partial C(\partial C/\partial z)$ amounts to $+0.48 \text{ N m}^{-2}$ and the thermal contribution $\partial\gamma/\partial T(\partial T/\partial z)$ to -0.16 N m^{-2} , resulting in a surface tension gradient of $\partial\gamma/\partial z = +0.32 \text{ N m}^{-1}$. This indicates that in the solutal boundary layer δ_c , i.e., ≤ 1 mm above the interface, the convection is governed by the concentration dependence of the surface tension and the convective flow points away from the growth front. In the remaining 2.5 mm towards the center of the zone thermocapillary convection is dominant, having the opposite flow direction. The qualitative distribution of the surface tension gradients is shown in Fig. 7.

²The following considerations are based on a value for the temperature dependence of the surface tension of $\partial\gamma/\partial T = -0.08 \text{ mN m}^{-1} \text{ K}^{-1}$, obtained by sessile drop measurements for $\text{Ge}_{1-x}\text{Si}_x$ melts with $0 \leq x \leq 13$ at% Si [26,27].

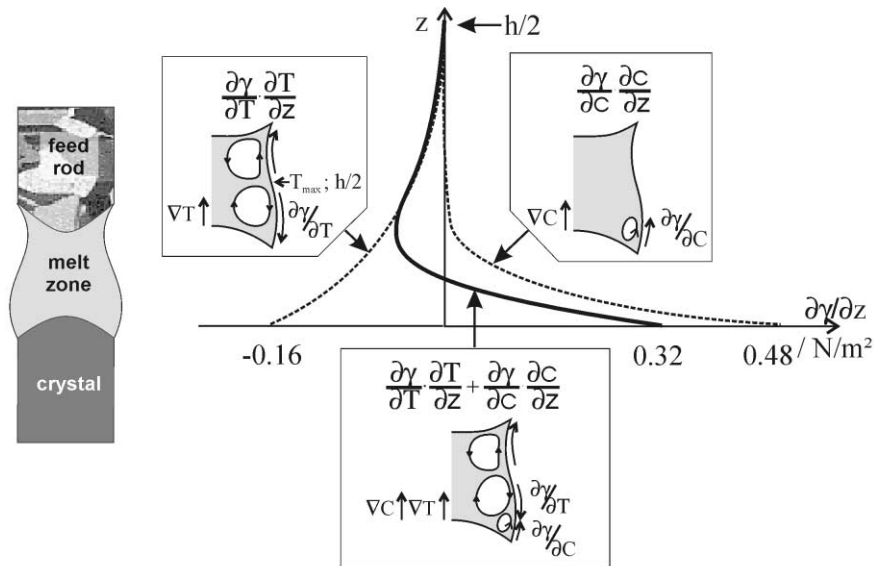


Fig. 7. Schematic profiles of the effective axial surface tension gradients and resulting flow rolls due to the thermocapillary and the solutocapillary dominated regions.

4. Summary

The main results can be summarized as follows: $\text{Ge}_{1-x}\text{Si}_x$ single crystals were grown reproducibly by the FZ method using a monoellipsoid mirror furnace. A maximum silicon concentration of 10 at% was achieved by using pre-synthesized feed rods with gradually increasing Si content. Growing crystals with even higher silicon concentrations appears to be feasible. The macrosegregation can be classified in four different regions: (I) silicon-free growth at the beginning, (II) a linear increase of the silicon concentration with a constant slope, (III) a plateau region with constant concentration and (IV) the last solidified melt zone with reduced silicon concentration.

EPDs are significantly reduced in the FZ crystals in comparison to crystals grown with wall contact by the VB method [23] (FZ: $7 \times 10^3 - 2 \times 10^4 \text{ cm}^{-2}$, VB: $6 \times 10^4 - 1 \times 10^5 \text{ cm}^{-2}$).

A deviation from a regular convex interface morphology as a function of the silicon concentration has been observed. The fact that it occurred only in conjunction with free melt surfaces indicates that this is caused by solutal Marangoni

convection. The possible additional impact of solutal buoyancy convection cannot be quantified yet and has to be investigated by further experiments.

The area dominated by solutocapillary convection is more susceptible to morphological instabilities; if the growth velocity is increased above the critical value, the interface breakdown starts within this small part of the boundary layer.

Acknowledgements

The authors are indebted to L. Rees-Isele for ampoules and photographs, and to W. Drayer for maintaining mechanical and control systems. Furnace support provided by U. Kerat and S. Rothenbacher during sample synthesis is also appreciated. Financial support for a large part of the research was granted by the German Federal Minister of Education and Research (BMBF) through DLR under contract number 50WM9503 and by the DFG, "Deutsche Forschungsgemeinschaft," under project number Be896/7. The support of the Alexander von

Humboldt Foundation for the Research Fellowship granted to one of the authors (T.A.C.) is also sincerely appreciated.

References

- [1] M.S. Saidov, A. Yusupov, R.S. Umerov, J. Crystal Growth 52 (1981) 514.
- [2] E.A. Fitzgerald, in: B.W. Wessels, E.N. Kaufmann, J.A. Giordmaine, J.B. Wachtman Jr. (Eds.), *Ann. Rev. Mat. Sci.* 25 (1995) 417.
- [3] J. Schilz, V.N. Romanenko, J. Mater. Sci. Mater. Electron. 6 (1995) 265.
- [4] R.H. Deitch, S.H. Jones, J.T.G. Digges, J. Electron. Mater. 29 (9) (2000) 1074.
- [5] E.A. Brandes, G.B. Brook, *Smithells Metals Reference-book*, 7th Edition, Butterworth-Heinemann Ltd., London, 1992.
- [6] M. Langen, T. Hibiya, M. Eguchi, I. Egry, J. Crystal Growth 186 (1998) 550.
- [7] J. Wollweber, D. Schulz, W. Schröder, J. Crystal Growth 163 (1996) 243.
- [8] J. Wollweber, D. Schulz, W. Schröder, J. Crystal Growth 158 (1996) 166.
- [9] O.N. Gromova, *Fizika i khimiiya obrabotki materialov* 5 (1968) 166.
- [10] A. Cröll, W. Müller-Sebert, K.W. Benz, R. Nitsche, *Microgravity Sci. Technol.* III/4 (1991) 204.
- [11] P. Dold, A. Cröll, K.W. Benz, J. Crystal Growth 183 (1998) 545.
- [12] M. Jurisch, J. Crystal Growth 102 (1990) 223.
- [13] D. Schwabe, J. Metzger, J. Crystal Growth 97 (1989) 23.
- [14] D. Schwabe, X. Da, A. Scharmann, J. Crystal Growth 166 (1996) 483.
- [15] K. Arafune, T. Kamei, A. Hirata, *International Astronautical Congress*, IAF-98-J.4.07, Melbourne, Australia, 1998.
- [16] K. Arafune, A. Hirata, J. Crystal Growth 197 (1999) 811.
- [17] P. Tison, D. Camel, I. Tosello, J.-J. Favier, *Proceedings of the First International Symposium on Hydromechanics and Heat/Mass Transfer in Microgravity*, Perm/Moscow, 1991, pp. 121–131.
- [18] S. Kaddeche, H.B. Hadid, D. Henry, J. Crystal Growth 141 (1994) 279.
- [19] A. Barz, *Züchtung von GeSi-Mischkristallen*, Ph.D. Thesis, Kristallographisches Institut, Albert-Ludwigs-Universität Freiburg, 1999.
- [20] W.A. Tiller, K.A. Jackson, J.W. Rutter, B. Chalmers, *Acta Metal.* 1 (1953) 428.
- [21] J.P. Dismukes, W.M. Yim, J. Crystal Growth 22 (1974) 287.
- [22] A. Cröll, *Floating-zone growth: the influence of process parameters and external fields*, Habilitation Thesis, Kristallographisches Institut, Albert-Ludwigs-Universität Freiburg, 1996.
- [23] P. Dold, A. Barz, S. Recha, K. Pressel, M. Franz, K.W. Benz, J. Crystal Growth 192 (1998) 125.
- [24] G. Müller, A. Ostrogorsky, in: D.T.J. Hurle (Ed.), *Handbook of Crystal Growth*, Vol. 2b, Elsevier Science Publishers, North-Holland, Amsterdam, London, New York, Tokyo, 1994, pp. 709–819.
- [25] N. Kaiser, A. Croell, F.R. Szofran, S.D. Cobb, K.W. Benz, J. Crystal Growth, 2001, accepted for publication.
- [26] P. Dold, N. Kaiser, K.W. Benz, A. Cröll, F.R. Szofran, S. Cobb, M. Volz, M. Schweizer, *51st International Astronautical Congress*, IAA-00-IAA.12.3.08, Rio de Janeiro, Brazil, 2000, pp. 1–11.
- [27] A. Croell, N. Kaiser, S.D. Cobb, F.R. Szofran, J. Crystal Growth, 2001, to be submitted.
- [28] Y. Takamura, T. Aoyama, K. Kuribayashi, *Proceedings of the Spacebound'97*, Montreal, Canada, 1997, pp. 229–235.
- [29] V.M. Glazov, S.N. Chizhevskaya, N.N. Glagoleva, *Liquid Semiconductors*, Plenum Press, New York, 1969.
- [30] H. Kölker, J. Crystal Growth 50 (1980) 852.
- [31] M. Langen, T. Hibiya, M. Eguchi, I. Egry, *18th Japanese Thermophysical Property Symposium*, 1997.
- [32] S.C. Hardy, J. Crystal Growth 69 (1984) 456.
- [33] S. Kimura, K. Terashima, J. Crystal Growth 180 (1997) 323.
- [34] P.H. Keck, W.V. Horn, *Phys. Rev.* 91 (1953) 512.
- [35] S.N. Zadumkin, *Sov. Phys. Solid State* 1 (1959) 516.